

Supplementary Information

Chelation Assisted Exfoliation of Layered Borides towards Synthesizing Boron based Nanosheets

*Asha Liza James and Kabeer Jasuja**

Discipline of Chemical Engineering, Indian Institute of Technology Gandhinagar, Palaj, Gujarat
382355, India

Corresponding Author

*Email: kabeer@iitgn.ac.in; Phone: +91-7874946373; Fax: +91-792397 2324

Section I: Crystal Structure of Layered Borides

Section II: Functionalized Nanosheets derived from MgB_2

Section III: Functionalized Nanosheets derived from AlB_2

Section IV: Evidence for Exfoliation

Section I: Crystal Structure of Layered Borides

1. CRYSTAL STRUCTURE OF MAGNESIUM DIBORIDE AND ALUMINIUM DIBORIDE
Metal diborides possess hexagonal “ AlB_2 -type” layered crystal structure, with $P6\ mmm$ symmetry. In these compounds, boron atoms are present in honeycomb layers, alternated with hexagonal layers of metal atoms. Mainly, diborides of main group (e.g.: Mg, Al) and rare earth metals (e.g.: Ti, Cr, Hf) crystallize in this kind of structure.

The structure of metal diborides showing the graphenic boron layers between hexagonal metal atom layers is represented below:

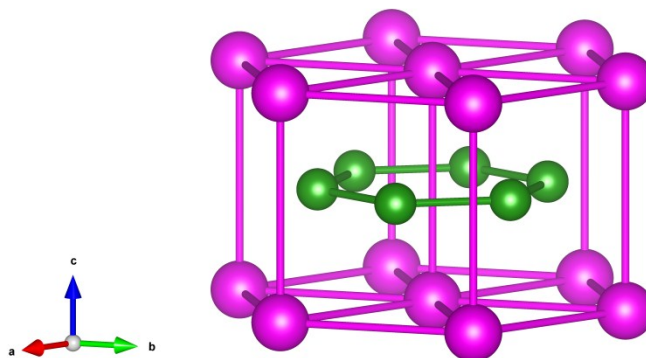


Figure S0. Crystal structure of layered metal diborides; green atoms represent boron and pink atoms represent metal atoms.

2. LATTICE PARAMETERS OF MAGNESIUM DIBORIDE

Table S1. Table showing lattice parameters and atomic distances in MgB_2

Lattice parameter a	0.3088 nm
Lattice parameter c	0.3524 nm
B-B distance	0.1783 nm
Mg-B distance	0.2506 nm

3. LATTICE PARAMETERS OF ALUMINIUM DIBORIDE

Table S2. Table showing lattice parameters in AlB_2

Lattice parameter a	0.3009 nm
Lattice parameter c	0.3262 nm

Section II: Functionalized Nanosheets derived from MgB₂

1. SUPPORTING TEM AND HRTEM IMAGES

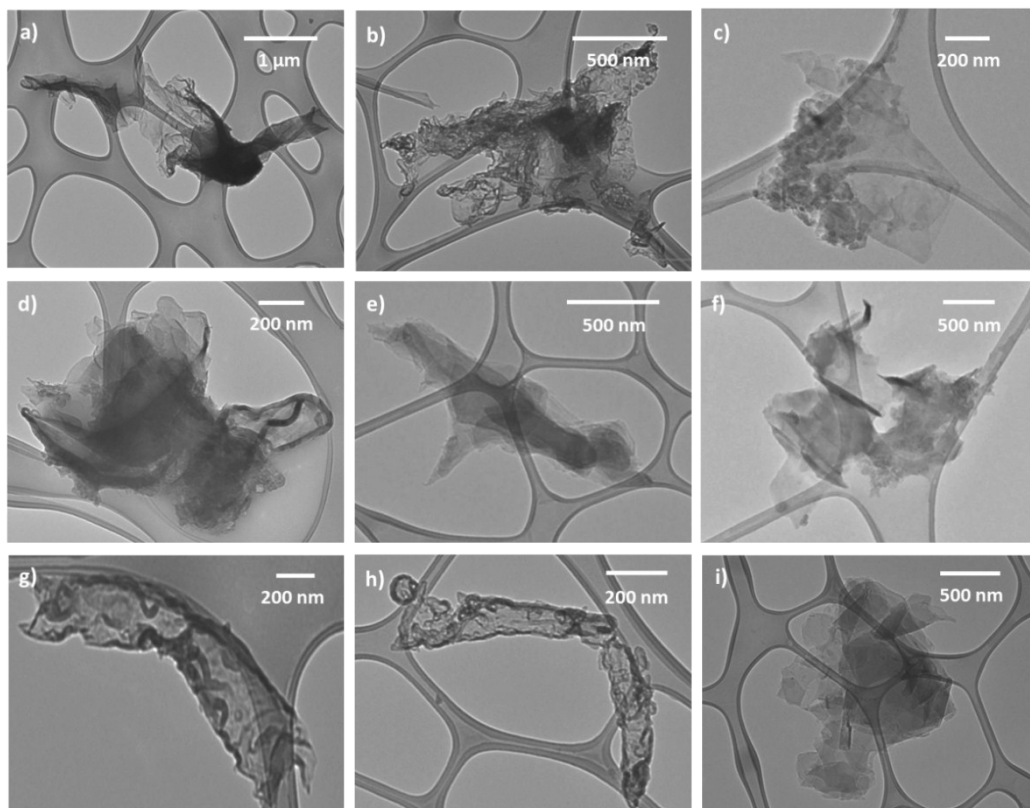


Figure S1. TEM images depicting various morphologies of the nanosheets with varying degrees of crumpling and rolling up.

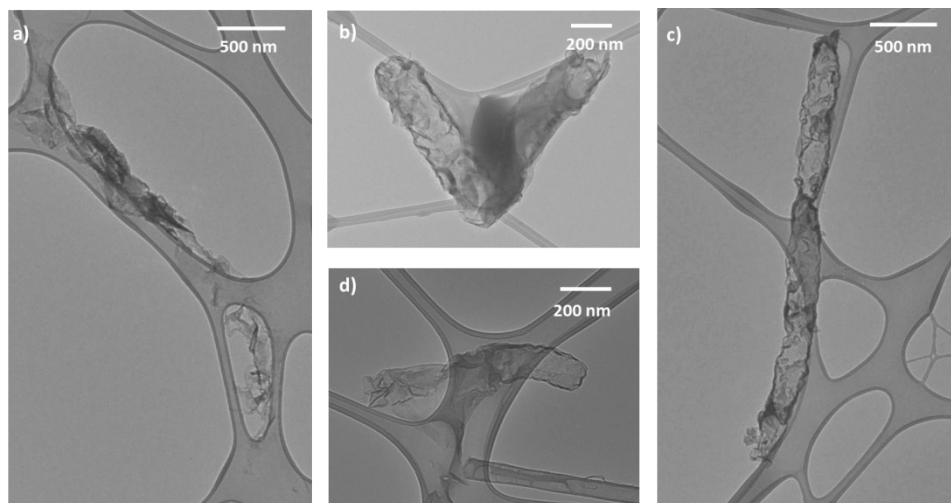


Figure S2. TEM images depicting more curled up and scrolled up morphologies of the nanosheets.

The chelation assisted exfoliation of MgB_2 yields aqueous colloidal dispersions of boron based nanosheets. TEM and HRTEM studies have revealed the size and morphology of the nanosheets. The lateral dimensions range from few hundred nanometers to well over few micrometers. The nanosheets exhibit moderate to highly crumbled morphology and tend to fold or roll onto them. HRTEM studies have also shown that these are few-layer-thick.

The colloidal dispersions of nanosheets were found to be stable over several weeks, without any visible signs of aggregation or precipitation. The Zeta potential values (measured using Malvern Zeta sizer Nano ZS) of the nanosheet dispersions were found to be around -24.85 mV, likely due to the ionization of functional groups present on nanosheets. As laid out by the chemical characterization, these nanosheets have significant oxy-functionalization. Boron oxides are known to have high affinity towards water, besides being very soluble in aqueous medium. This could be another reason for the stability and excellent dispersibility of the nanosheets in water.

Lyophilizing 12ml of the aqueous dispersions resulted in ~4mg of white fluffy powder; the yield was hence calculated to be about 7.2%. This powder sample of nanosheets was analyzed under FESEM.

As explained in Supporting Information Section I, MgB_2 has an interlayer spacing of 0.3524 nm (the c parameter). So if we consider Figure 2e and 2f in the manuscript, a nanosheet with a thickness of < 2nm would correspond to $\sim (2 \text{ nm}/0.3524 \text{ nm}) \approx 5$ to 6 layers. This would only be a rough estimate because, a lot many Mg atoms would have been displaced with oxy/hydroxyl/hydride functionalization happening at these sites, thereby changing the interlayer spacing values in the nanosheets as opposed to the parent boride crystals. But, it agrees well with the AFM results presented in the manuscript, wherein the nanosheets have been found to be 1.0-1.7 nm thick as seen from the AFM histogram presented in Figure S5.

It had been extremely challenging to image these nanosheets under HRTEM as they were getting charged and were unstable under the electron irradiation. Especially, thin edges of the nanosheets were found to be difficult to image under HRTEM, due to charging. Hence most HRTEM images depict the transverse view of folded edges with many layers. Atomic resolution imaging of few layered structures has been reported to be difficult as they are highly sensitive to the electron beam radiation.¹ Cretu *et al.* have shown that insulating materials like *h*-BN nanosheets suffer electron irradiation damage due to electrostatic charging.²

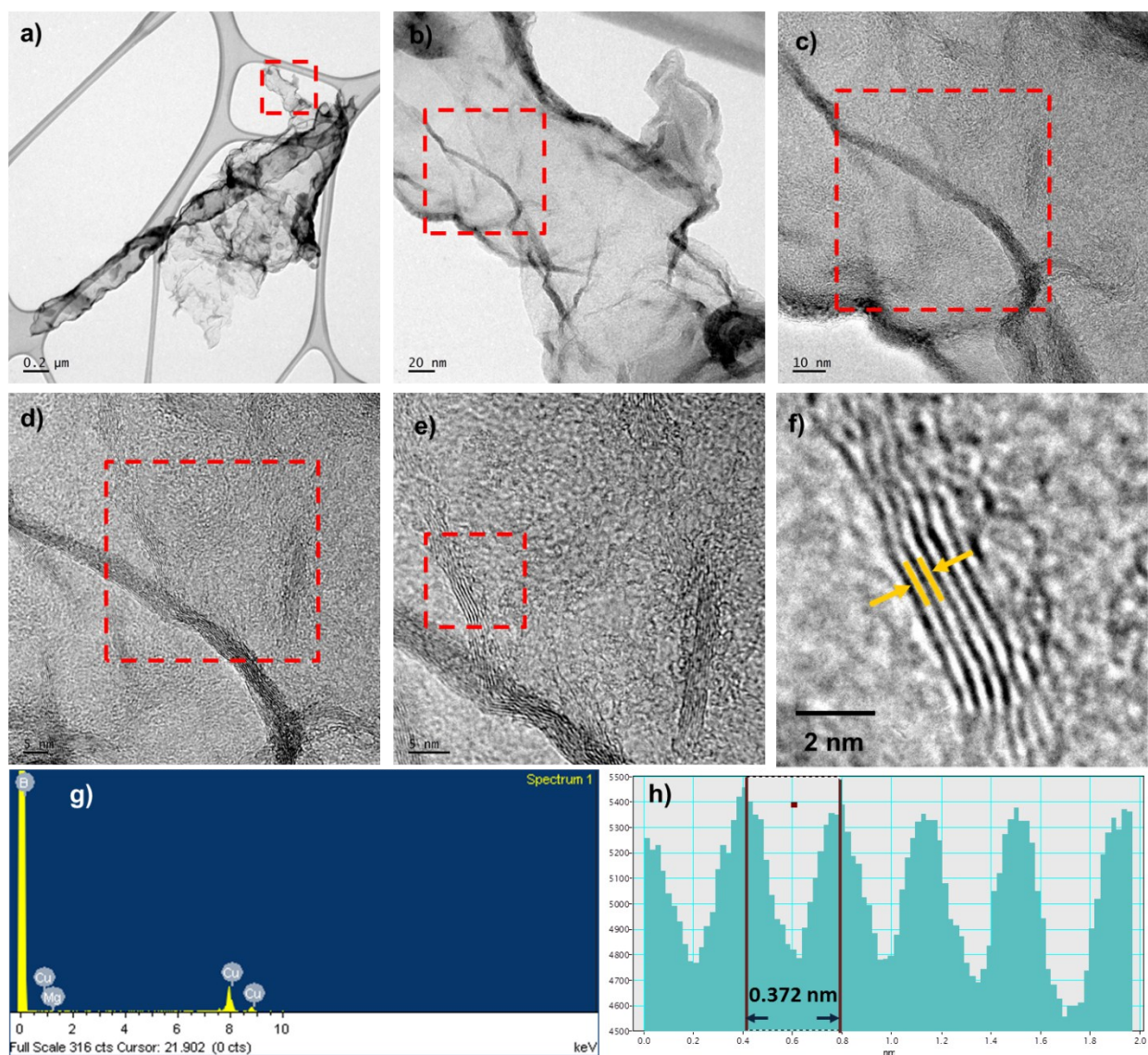


Figure S3. HRTEM images depicting - (a) a highly crumpled nanosheet; (b) zoomed image of the top part of the nanosheet; (c) zoomed image of the marked region in panel *b* showing several folds in the nanosheets that are zoomed upon in successive panels; (d,e, and f) transverse view of the fold marked in panel *e* showing it to be 5-6 layers thick; (g) EDX spectra acquired under HRTEM showing the nanosheet is chiefly composed of boron; (h) Line profile of the fold in nanosheet represented in panel *f* indicating the inter layer thickness to be ~ 0.37 nm; the lattice distortion effected by Mg loss and functionalization subsequent to exfoliation could have led to expansion of the layers (inter layer distance in parent MgB_2 being 0.3524 nm).

The following panel show a series of zoomed in images of a thicker folded edge comprising of 12 layers. The edge can be measured to be approximately 4.2 nm thick, and as per our previous calculations this corresponds to $\sim (4.2 \text{ nm}/0.3524 \text{ nm}) \approx 12$ layers.

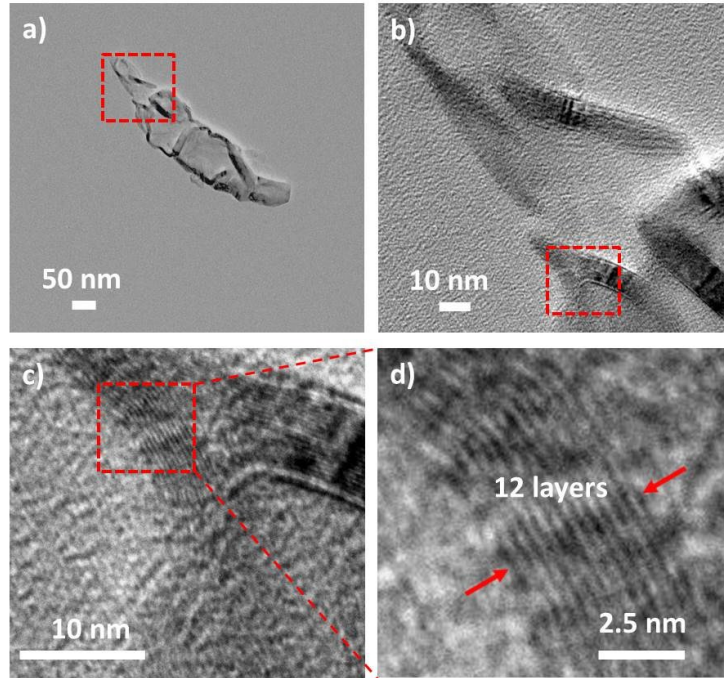


Figure S4. HRTEM images depicting - (a) a nanosheet with folded edges; (b-c) Zoomed in images of the region marked in red in panel *a* ; (d) the transverse view of nanosheet edge clearly shows the few-layer-thick nature.

2. THICKNESS DISTRIBUTION FROM AFM

The AFM studies revealed the nanosheet thicknesses to lie in the range ~ 1.0 - 1.7 nm. The following histogram shows the thickness distribution of the nanosheets.

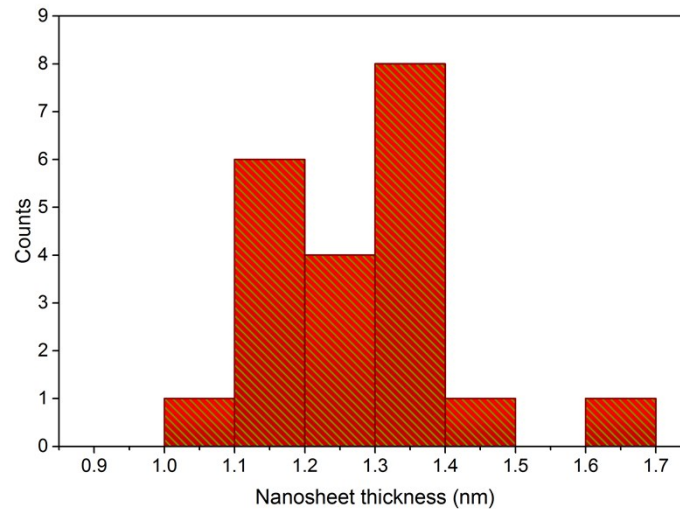


Figure S5. Thickness distribution of the MgB_2 derived nanosheets from AFM

3. SUPPORTING FE-SEM IMAGES

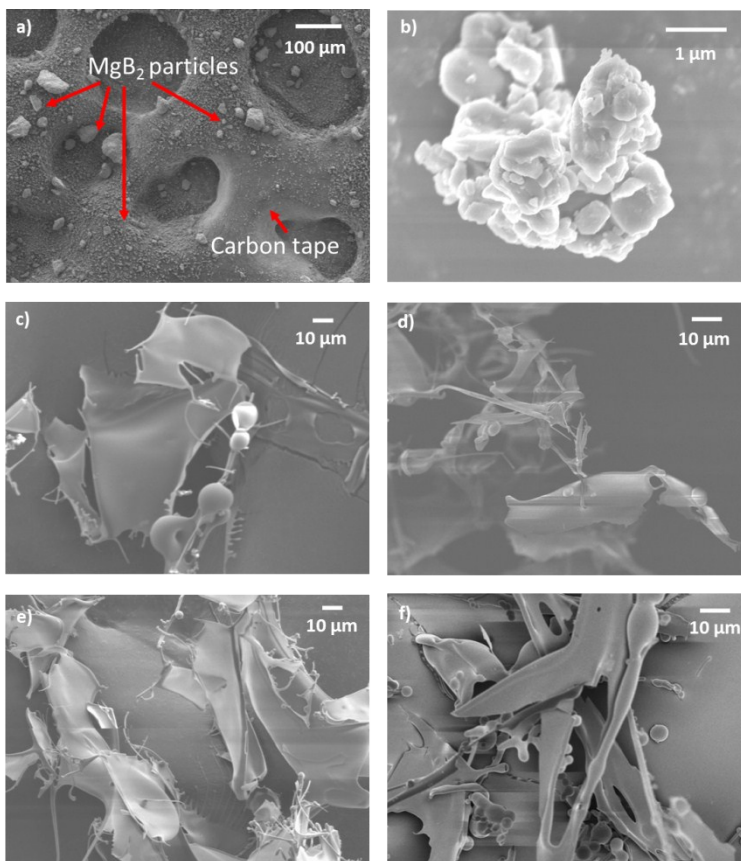


Figure S6. FE-SEM images showing (a-b) standard MgB₂ crystals, a) represents low magnification image of MgB₂ dusted onto adhesive carbon tape showing different particle sizes and b) represents a particle of ~ 2 μm size; (c-f) the lamellar nature of the nanostructures present in the powder obtained from the lyophilization of colloidal dispersion. Rod shaped appendages and spherical protrusions are also observed. Such protrusions are thought to result from evolution of gases due to exfoliated nanosheet-water interactions.

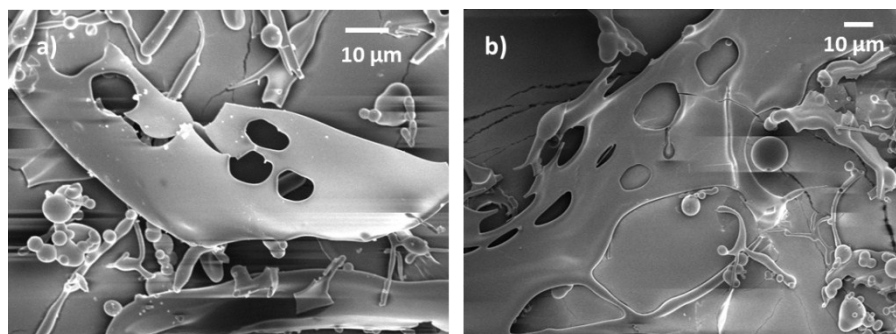


Figure S7. FE-SEM images of lyophilized nanosheet sample showing the scattered spherical structures and the presence of perforations; evolved gases likely lead to bulging (hence the spherical protrusions) and subsequent rupture that creates these pores.

4. SAMPLE CALCULATIONS FOR ICP-AES:

Inductively Coupled Plasma-Atomic Electron Spectroscopy (ICP-AES) gives the elemental concentrations in mg/ml of Mg and B in the aqueous dispersion of nanosheets. Ultrapure Millipore water (Type I) is used as control. The molar concentration of the element can be found upon dividing its elemental concentration (as obtained from ICP results) by its atomic weight.

The Mg:B stoichiometric ratio is calculated as:

$$\frac{\text{Elemental concentration of Mg}}{\text{Atomic weight of Mg (24.305)}} : \frac{\text{Elemental concentration of B}}{\text{Atomic weight of B(10.811)}}$$

For example, sample 1 has 32.225 mg/ml Mg and 55.075 mg/ml B. Hence, the Mg:B ratio is **0.52:2** as shown below:

$$\frac{32.225}{24.305} : \frac{55.075}{10.811} = \frac{0.52}{2}$$

The Mg:B ratio for the standard sample was found out to be 0.98:2, by comparing the XRD pattern for pristine MgB₂ with the ICSD database (PDF 01-076-9004).

5. FESEM-EDX FOR QUALITATIVE CHEMICAL COMPOSITION

EDX spectra were collected under FESEM for both MgB₂ and the nanosheets and compared. We acknowledge that for lighter elements and especially boron, EDX is not recommended for quantification of chemical composition. Still, the data provides a qualitative idea about the system. Carbon signal originates from the adhesive tape on the stub onto which the powders are dusted as well as from contamination. The Mg-deficiency owing to selective extraction by the chelant molecules as well as the oxy-functionalization in the nanoscaled version is clearly evident from the data. The moderate boron signal in the nanosheets sample is probably due to the following reasons - (i) the very thin nature of the nanosheets sample, (ii) X-rays emitted from B shells have low energy and hence get absorbed by the sample before reaching the detector, (iii) overlap of K α peak of boron with that of carbon gets more pronounced due to much higher amount of carbon present from the tape and/or contamination which may lead to lesser B signal.

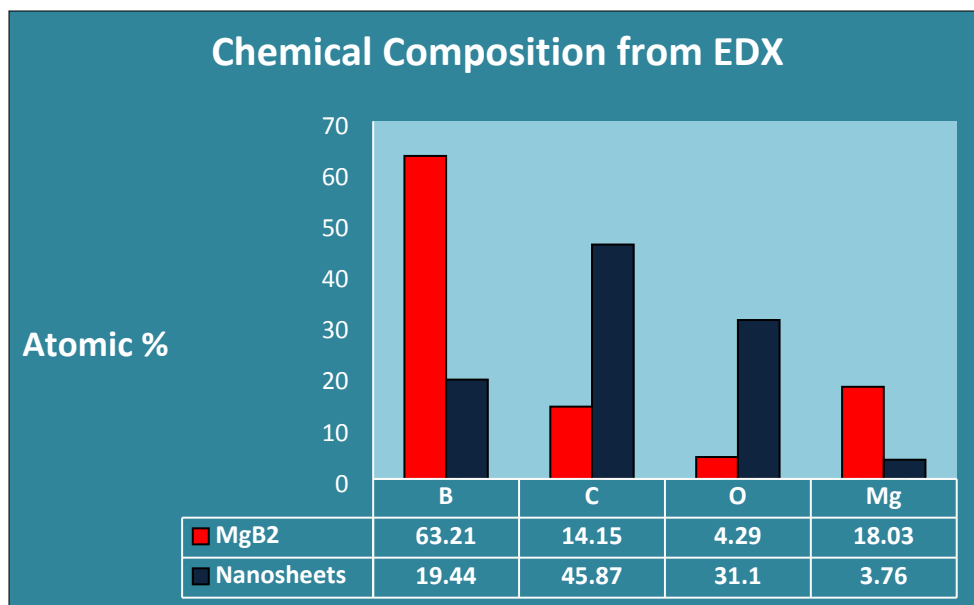


Figure S8. FESEM-EDX data for MgB₂ vs nanosheets showing chemical composition; the Mg deficiency and oxy functionalization in the nanosheets are clearly seen.

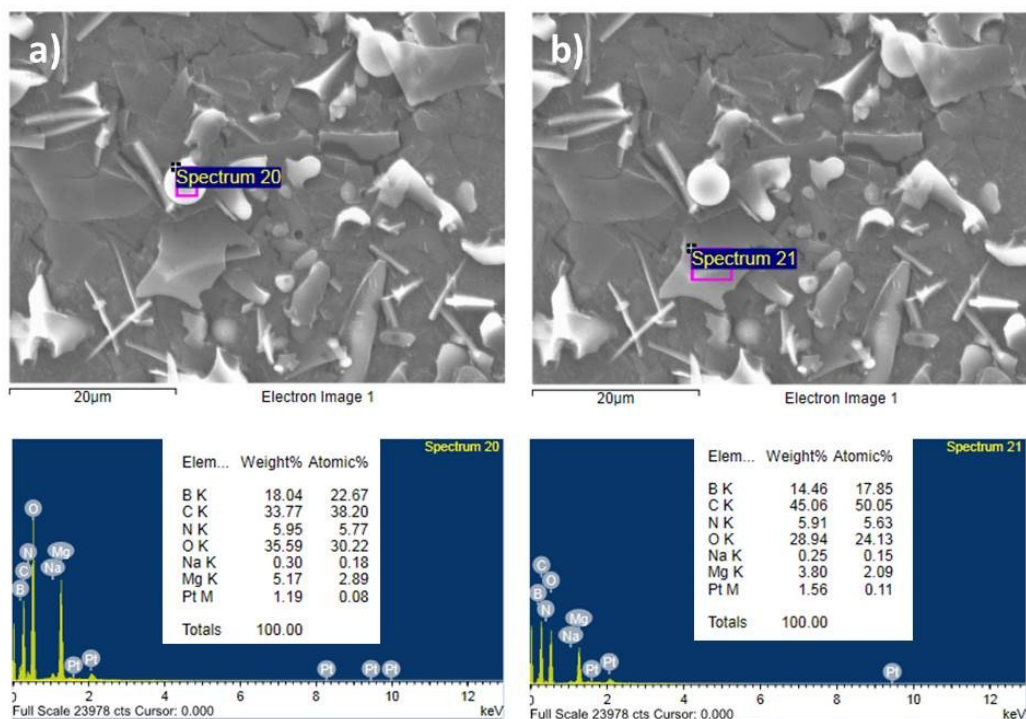


Figure S9. EDX spectra from different sites on the same FE-SEM image of lyophilized nanosheet sample showing sheet like and spherical nanostructures; both these structures show similar chemical composition and are “boron rich” as evident from the EDX spectra. The Mg:B ratio from both structures are also similar.

6. SOLID STATE NMR SPECTROSCOPY

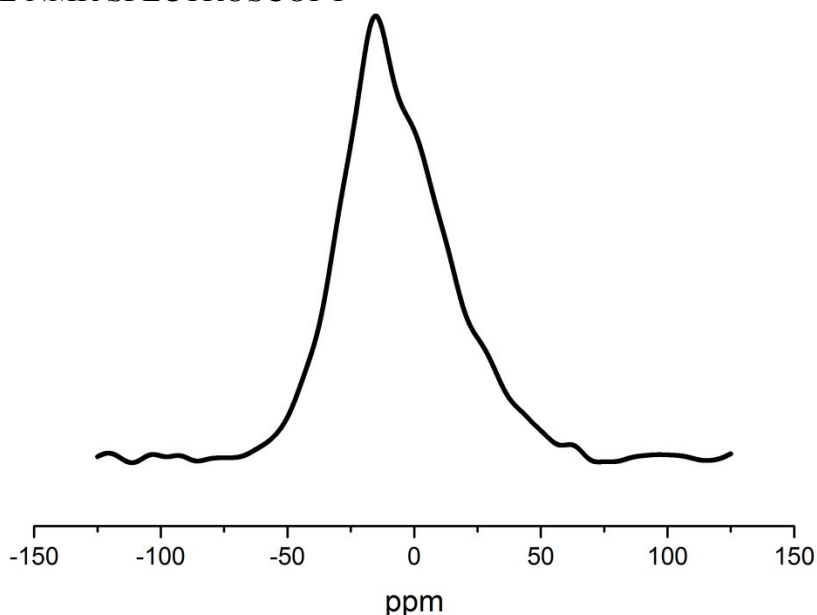


Figure S10. ^{11}B solid state NMR spectrum for the MgB_2 derived nanosheets suggests the presence of borohydride species.

The NMR spectrum was acquired for the lyophilized form of the nanosheets derived from MgB_2 . The spectrum is found to consist of a broad peak (spanning from -50 ppm to +50 ppm) centered around -15 ppm. The peak at -15 ppm indicates the presence of $[\text{B}_x\text{H}_y]^{n-}$ species as demonstrated by Gupta *et al.*, signifying the presence of hydride functional groups.³ Pistidda *et al.*, have also reported in their paper on high pressure ball milling of MgB_2 in hydrogen environment, a similar broad peak between 20 to -30 ppm with shoulders at 0.53 ppm and -15.57 ppm, attributed to a mixture of several $\text{Mg}(\text{B}_n\text{H}_m)_y$ species.⁴ The extremely broad peak in our work may also suggest the presence of an ensemble of other species including hydroxyl and oxy functionalized boron contributing to shoulder peaks. For example, the shoulder peak near 0 ppm may be attributed to tetrahedral BO_4 species.⁵

7. RAMAN SPECTROSCOPY

Figure S11 depicts the Raman spectra of pristine MgB_2 and nanosheets, both exhibiting peaks in the region $\sim 550\text{-}650\text{ cm}^{-1}$, confirming the presence of planar B-B bonds. The Raman active E_{2g} mode, typically observed in this range corresponds to the in-plane, antiphase stretching, and hexagon-distorting displacement of boron atoms.⁶ Compared to standard MgB_2 , the peaks displayed in the Raman spectrum of nanosheets in this region, are shifted to higher energies. A comparable shift to higher energies has been reported by Awana *et al.* as a result of disordered substitution on the MgB_2 lattice.⁷ Similar shifts of E_{2g} modes to higher energies have also been reported in graphene upon functionalization.⁸ In addition, a peak near 751 cm^{-1} is

observed in the nanosheets sample, which has been reported in MgB_2 to be linked to the phonon density of states due to disorder.^{9,10,11} Thus, the functionalization, which leads to modified boron planes, is expected to create disorder in the boron hexagonal layers, thereby causing a shifting of in plane vibrational E_{2g} phonon frequencies.⁷ Yates *et al.* have reported that defects introduced by alloying oxide impurities into the boron planes get reflected in the E_{2g} frequencies.¹² It is relevant to note here, that a lot of disparities exist in the current literature pertaining to the Raman spectroscopy studies on MgB_2 as pointed out by Alarco *et al.* in their review of phonon modes in MgB_2 .⁶ In addition, the multitude of functional groups that boron can form in varying degrees makes Raman analysis of the nanosheets a challenging task. Further analysis is required to ascertain the details of the other Raman features; we hope to accomplish this in the near future.

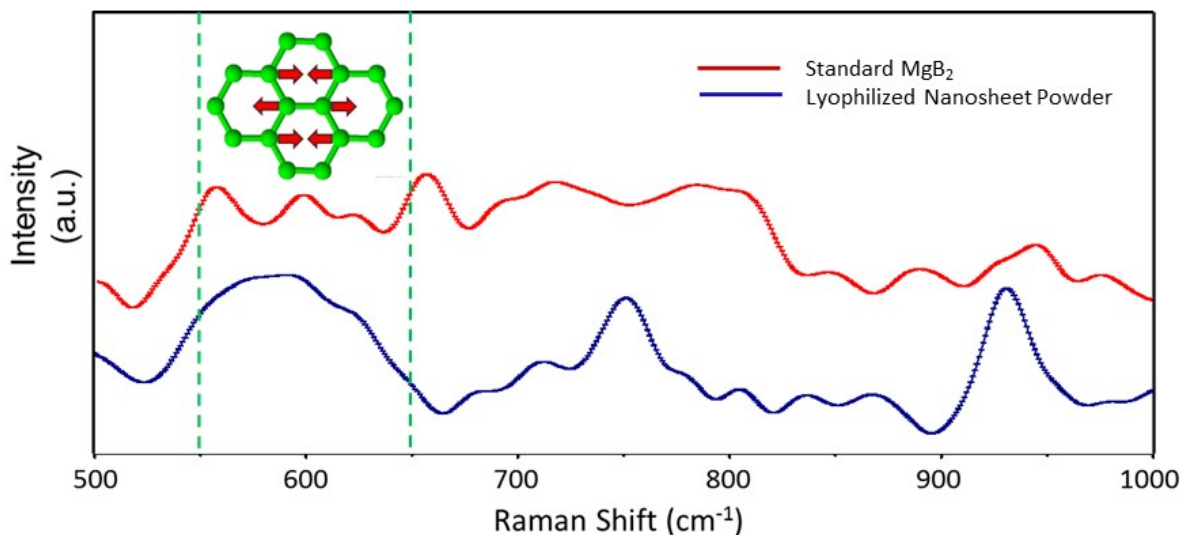


Figure S11. Raman spectra of the standard MgB_2 and lyophilized nanosheets sample. The Raman active E_{2g} mode is in the range of 550-650 cm^{-1} in MgB_2 . When compared to the standard sample, there is a shifting of peaks in the nanosheet sample, which can be corroborated to two dimensional confinement and functionalization. The inset figure depicts the in plane stretching vibrations of the boron atoms corresponding to the E_{2g} mode.

8. X-RAY PHOTOELECTRON SPECTROSCOPY

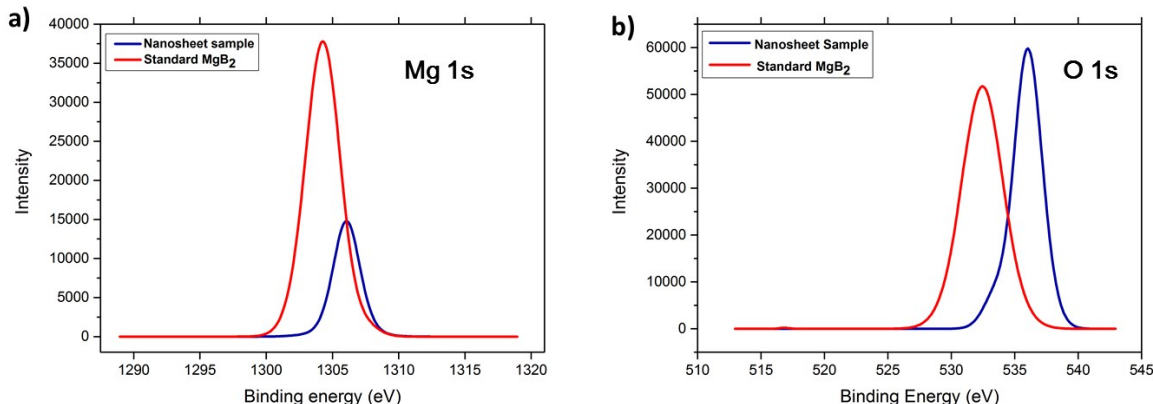


Figure S12. X-ray Photoelectron Spectroscopy results from standard MgB₂ and nanosheet sample (a) Mg 1s spectra, indicate a reduction in the amount of Mg in the nanosheets as compared to the standard MgB₂ as well as a shift to higher energies; (b) O 1s spectra, indicating a shift to higher energies in the nanosheets sample owing to the multitude of functional groups.

Mg 1s spectra are observed to shift to higher energies (from 1304.25 eV to 1306.05 eV) in the nanosheets sample as compared to the standard MgB₂. This is attributed to the presence of magnesium in a more oxidized form in the nanosheets as compared to the standard MgB₂.¹³

The 532.45 eV peak observed in the O 1s spectrum of standard MgB₂ can be attributed to surface oxygen or –OH chemisorbed to the MgO surface along with B₂O₃ phase as both MgO and B₂O₃ give peaks around 531-533 eV.^{13,14} The shift to higher binding energy (536.05 eV) observed in the nanosheets sample is jointly made up by the presence of oxygen-functionalized boron, hydroxyl species,¹⁵ and also the presence of silicon dioxide from the silica wafer substrate used to deposit the nanosheets dispersion. This is in agreement with the observation made by Talapatra *et al.* wherein they commented that oxygen attached to boron shows higher binding energy as boron is more electronegative than magnesium.¹³

9. OPTICAL STUDIES

The UV-Vis spectra of the (suitably diluted) dialyzed aqueous dispersions were obtained on a Jasco V-750 spectrophotometer. As observed from the spectrum, the nanosheet dispersions strongly absorb in the UV region, below 400 nm. Such a strong absorption in the far UV region (50-300 nm) was predicted for graphene-like hydroboron sheets by Wu *et al.* in their first principles study.¹⁶ Also, similar optical spectrum was displayed by the nanosheets synthesized in our previous work, wherein we attributed the peaks in the UV region to arise from $\pi \rightarrow \pi^*$ transitions and functionalization on the nanosheets.¹⁷ The optical bandgaps for both samples were calculated using the relation: $E = hc/\lambda$; where E is Band gap energy, h is the Planck's constant, c is the velocity of light, and λ is the cut-off wavelength, where absorption just starts.

The band gap value for nanosheets derived from MgB_2 was calculated to be 3.18 eV by observing the cut-off wavelength as 390 nm.

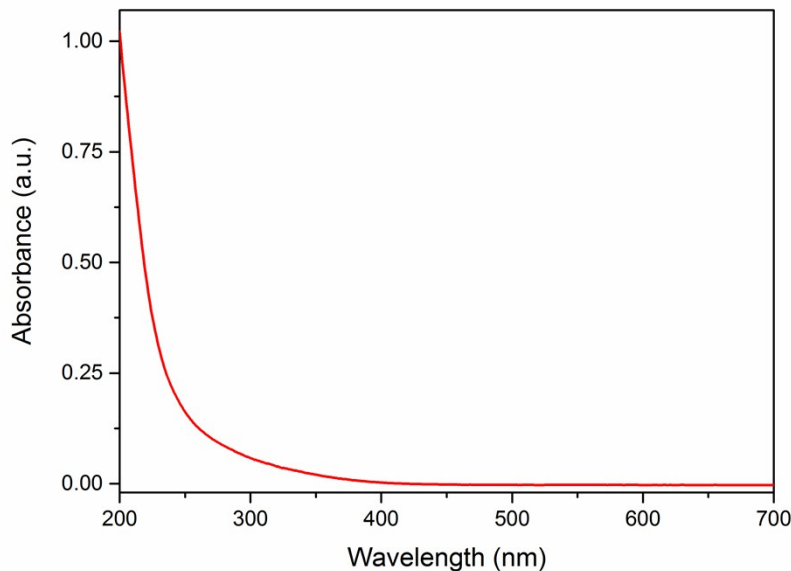


Figure S13. Optical spectrum of the aqueous dispersions of the functionalized nanosheets derived from MgB_2 showing high absorbance in the UV region.

10. SELECTED AREA ELECTRON DIFFRACTION (SAED) PATTERNS

The SAED patterns consist of diffuse rings, indicating the amorphous nature of the nanosheets, which can be ascribed to the presence of functional groups on their surface. This functionalization is also evidenced by the EDX, FTIR, and XPS results.

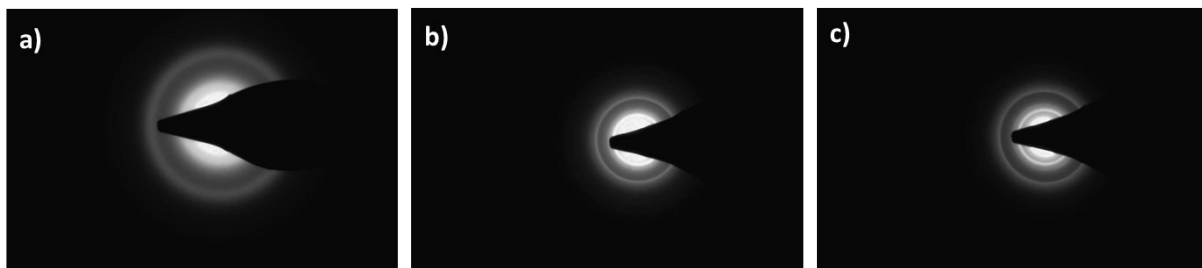


Figure S14. SAED patterns of the MgB_2 derived nanosheets indicate their amorphous nature, owing to lack of crystallinity due to the functionalization acquired upon exfoliation.

11. LATTICE DISTORTION IN NANOSHEETS:

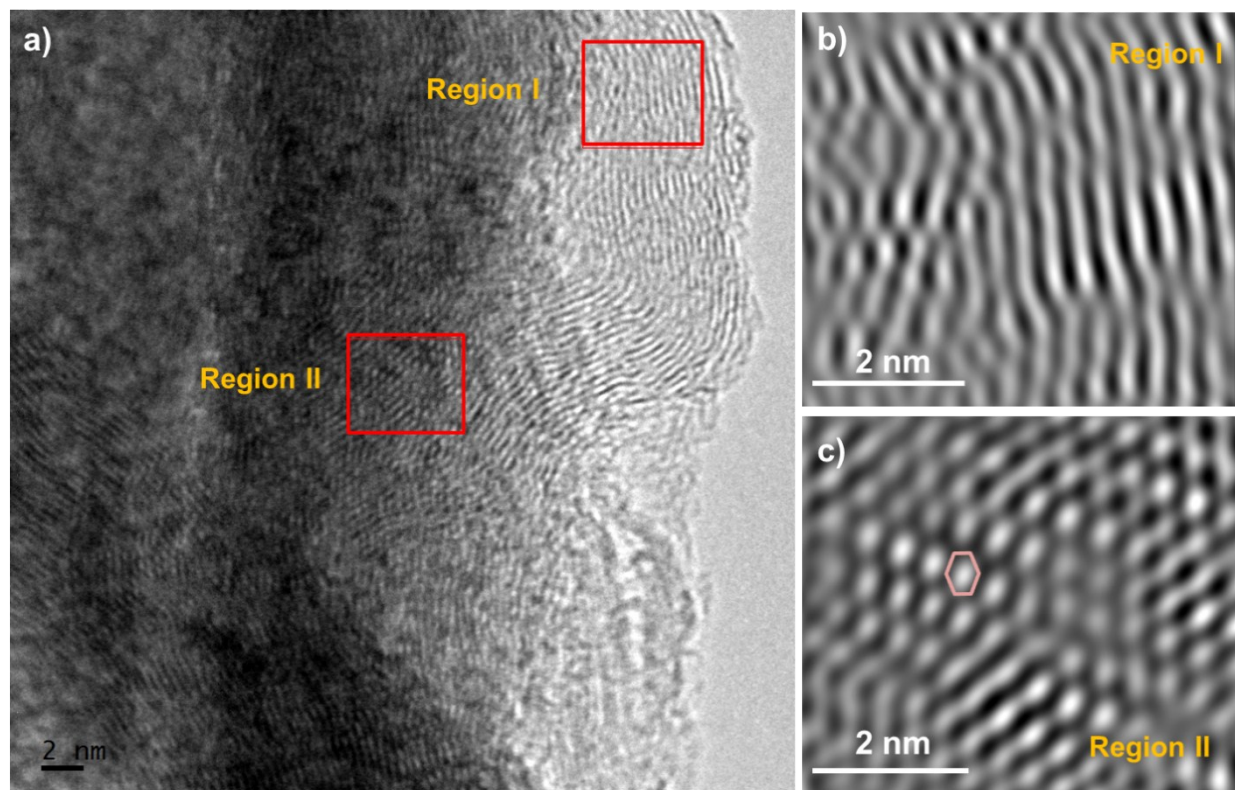


Figure S15. HRTEM image of a nanosheet edge (panel *a*) and the corresponding IFFT of the regions marked in red showing regions with distorted lattice (as shown in panel *b*) and localized regions of partly preserved hexagonal lattice (as shown in panel *c*). The loss of Mg and functionalization in the aqueous milieu upon exfoliation results in disorder and defects, thereby distorting the lattice in the nanosheets. Still, partly preserved hexagonal lattice is present in certain regions. These observations corroborate the insights gained from Raman spectroscopy results, wherein peaks corresponding to planar B-B bonds are present in the spectrum from the nanosheets although they are shifted, owing to disorder caused by functionalization.

12. X-RAY DIFFRACTION STUDIES:

The XRD analysis for the standard sample was performed on a diffractometer from Bruker AXS, Germany (D8 Discover). The XRD spectrum for the standard MgB_2 has been matched with the ICSD database with $\text{Mg}_{0.98}\text{B}_2$ (PDF 01-076-9004).

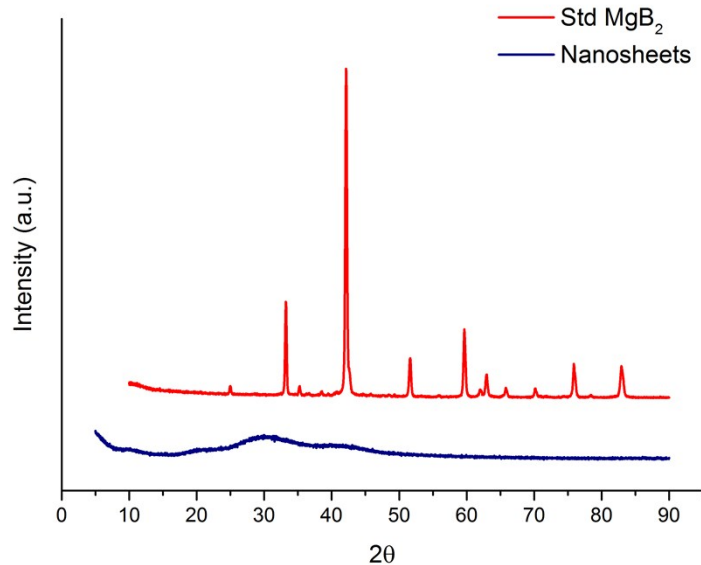


Figure S16. XRD pattern of standard MgB₂ and nanosheets; the peaks corresponding to the metal boride are absent in the nanosheet form.

13. EVIDENCE FOR METAL-CHELANT COMPLEX:

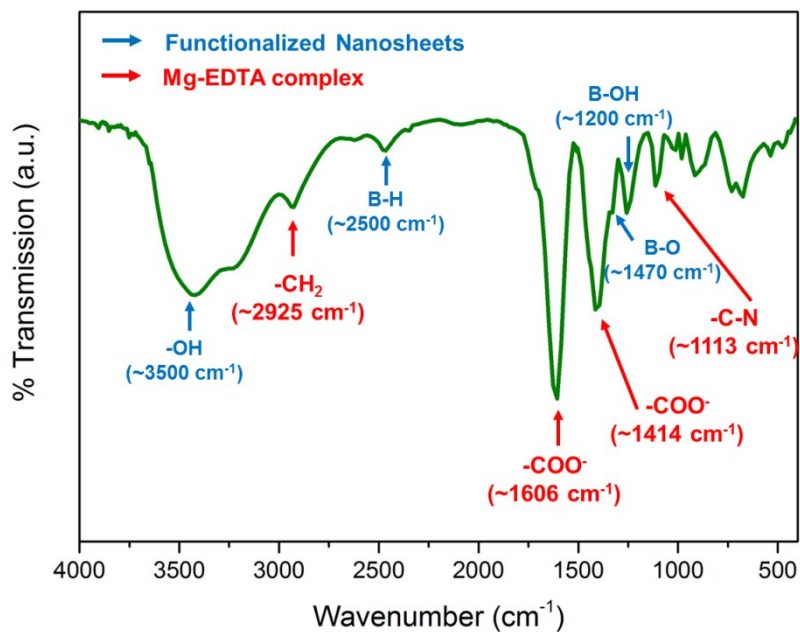


Figure S17. Evidence for chelation assisted exfoliation in terms of Mg-EDTA complex determination: FTIR spectrum of the lyophilized form of the supernatant recovered after centrifugation, showing peaks that affirm the presence of Mg-EDTA complex along with the functionalized nanosheets.

Section III: Functionalized Nanosheets derived from AlB_2

The yield of AlB_2 derived nanosheets:

The chelation assisted exfoliation of AlB_2 yields aqueous dispersions of boron based nanosheets. TEM and HRTEM studies have revealed the nanosheets to be very crumpled with a tendency to roll up. The lateral dimensions range from 2-5 micrometers. HRTEM studies have also shown that these are few-layer-thick.

Lyophilizing 10ml of the aqueous dispersions of nanosheets derived from AlB_2 resulted in ~2mg of pale white powder; the yield was hence calculated to be about 4.3%. The lyophilized powder was also analyzed under FE-SEM.

1. TEM IMAGES OF AlB_2 DERIVED NANOSHEETS

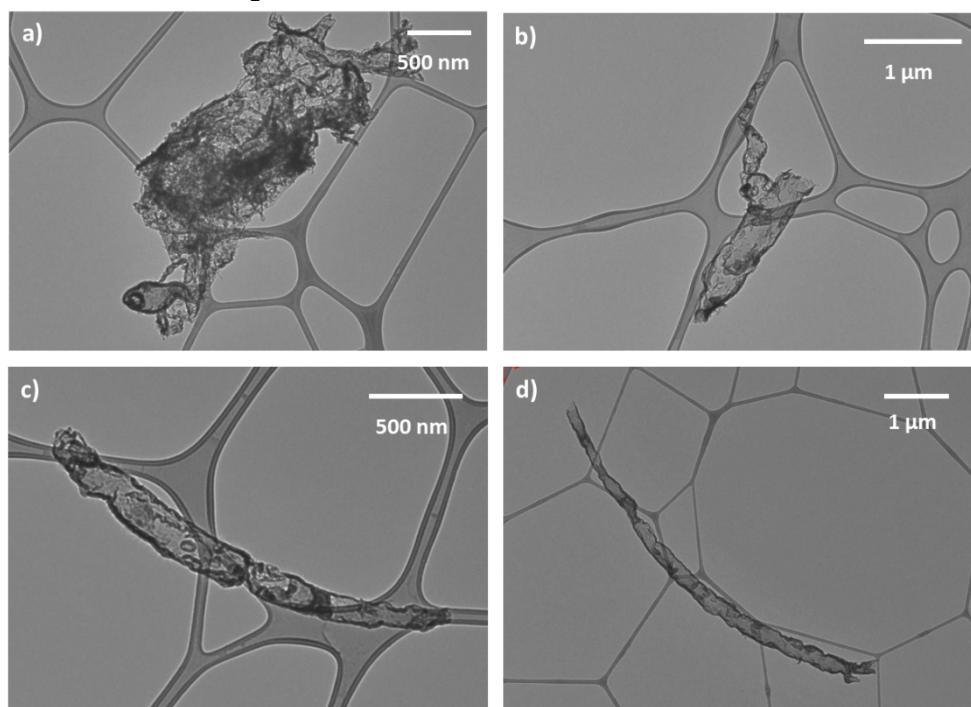


Figure S18. TEM images of extremely crumpled and self-wrapped nanosheets from chelation assisted exfoliation of AlB_2

2. HRTEM IMAGES OF AlB₂ DERIVED NANOSHEETS

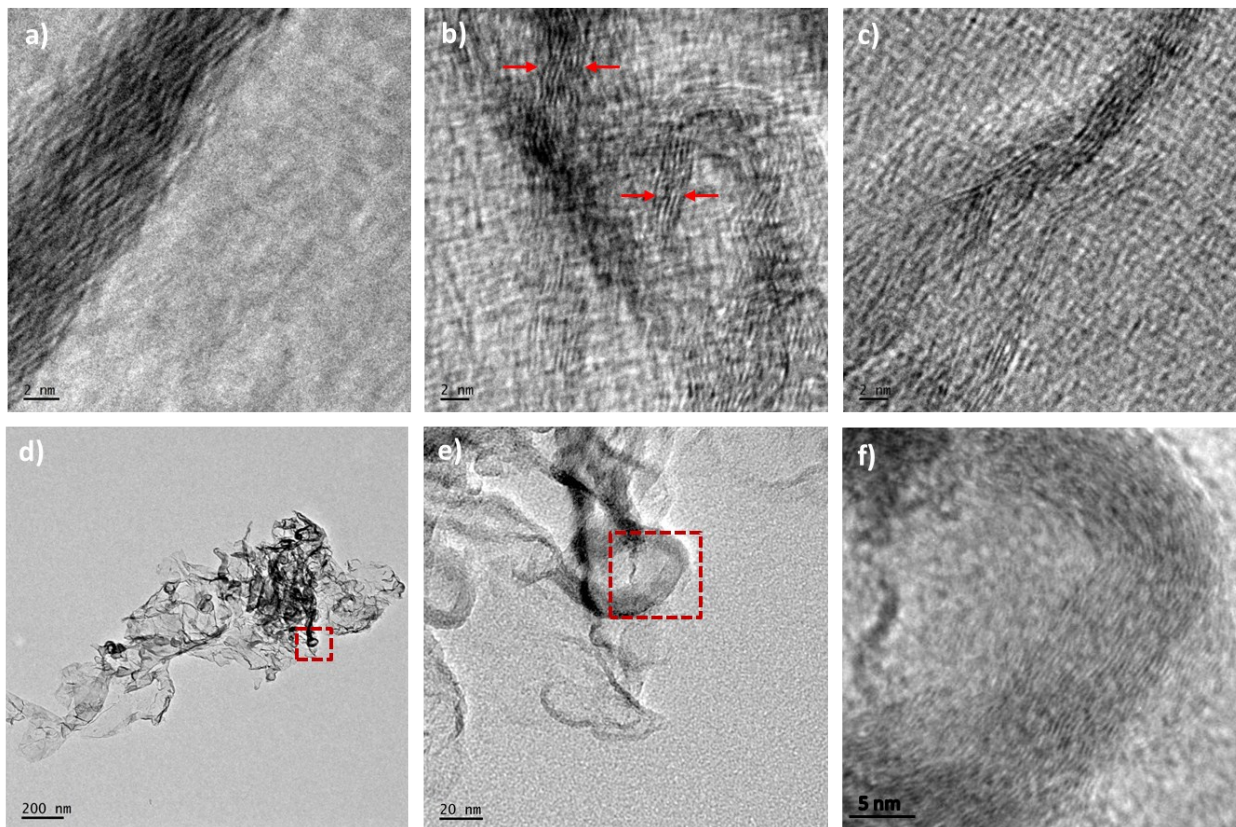


Figure S19. HRTEM images of nanosheets from chelation assisted exfoliation of AlB₂: the curved edge of the nanosheet in panel *d* has been zoomed out in panels *e* and *f*.

3. FESEM IMAGES OF AlB_2 DERIVED NANOSHEETS

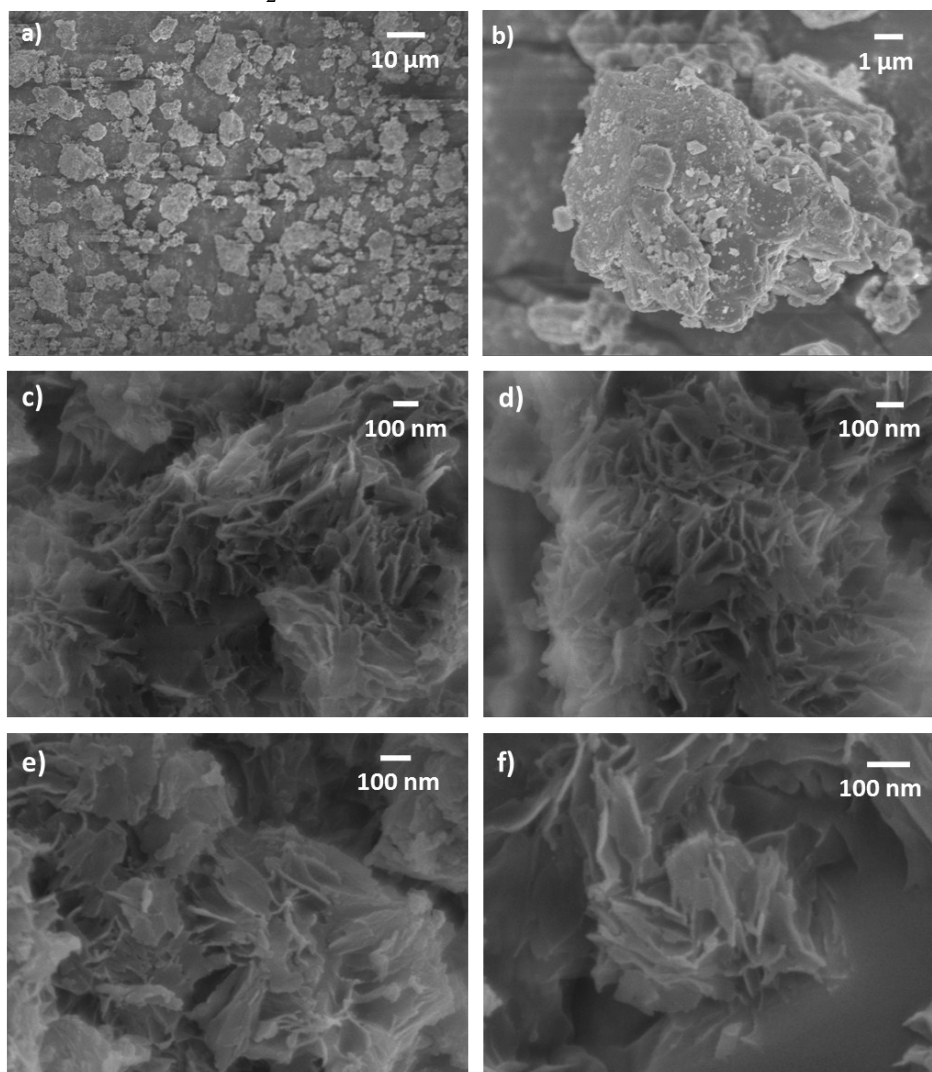


Figure S20. FESEM images of (a-b) standard AlB_2 and (c-f) AlB_2 derived nanosheets showing their aggregation into bunches.

4. ICP-AES CALCULATIONS

For the case of AlB_2 the calculation is as follows: the dialyzed nanosheet dispersion has 1.048 mg/ml Al and 42.844mg/ml B. Hence, the Al:B ratio is $\sim 0.02:2$ as shown below:

$$\frac{1.048}{26.981} : \frac{42.844}{10.811} = \frac{0.02}{2}$$

The Al:B ratio for the standard sample was found out to be 1:2, by comparing the XRD pattern for pristine AlB_2 with the ICSD database (PDF 00-010-0232). The XRD was performed on Bruker D8 Discover diffractometer.

5. XRD ANALYSIS

The XRD spectrum for the standard AlB_2 has been matched with the ICSD database (PDF 00-010-0232).

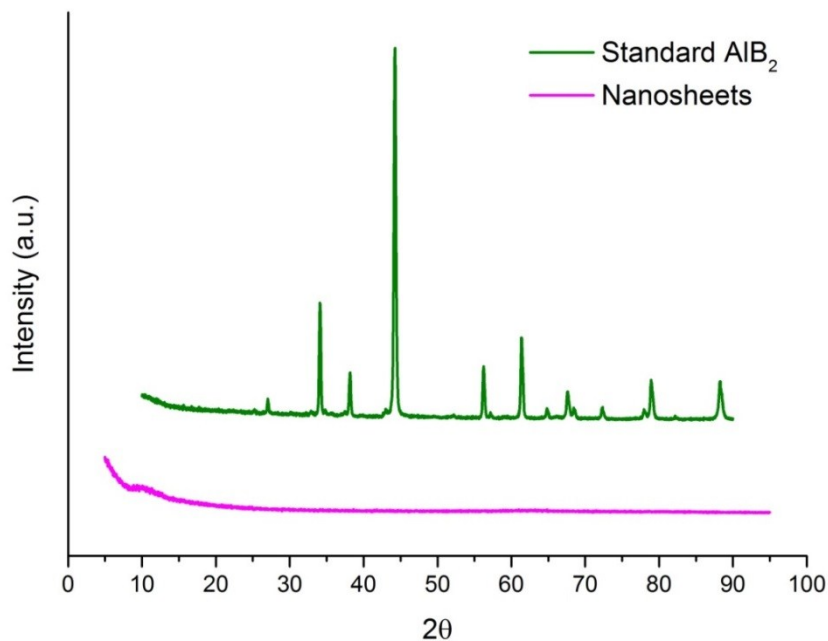


Figure S21. XRD pattern of standard AlB_2 and nanosheets; the peaks corresponding to the metal boride are absent in the nanosheet form.

6. SAED PATTERNS FOR AlB_2 DERIVED NANOSHEETS

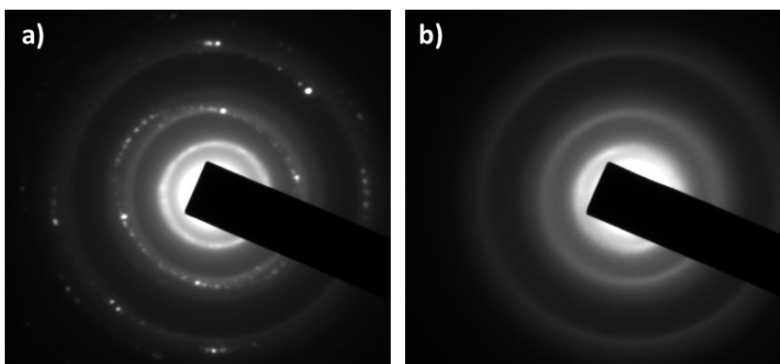


Figure S22. SAED patterns of the AlB_2 derived nanosheets - (a) Pattern with random spots and weak rings indicating poly crystallinity, the incidence of such patterns is very low; (b) Pattern with weak, diffuse rings indicating loss of crystallinity due to Al extraction and functionalization.

7. OPTICAL STUDIES

The UV-Vis spectra of the (suitably diluted) dialyzed aqueous dispersions were obtained on a Jasco V-750 spectrophotometer. The nanosheet dispersions derived from AlB_2 also strongly absorb in the UV region, below 400 nm. The band gap value for nanosheets derived from AlB_2 was calculated as 3.63 eV by observing the cut-off wavelength as 342 nm.

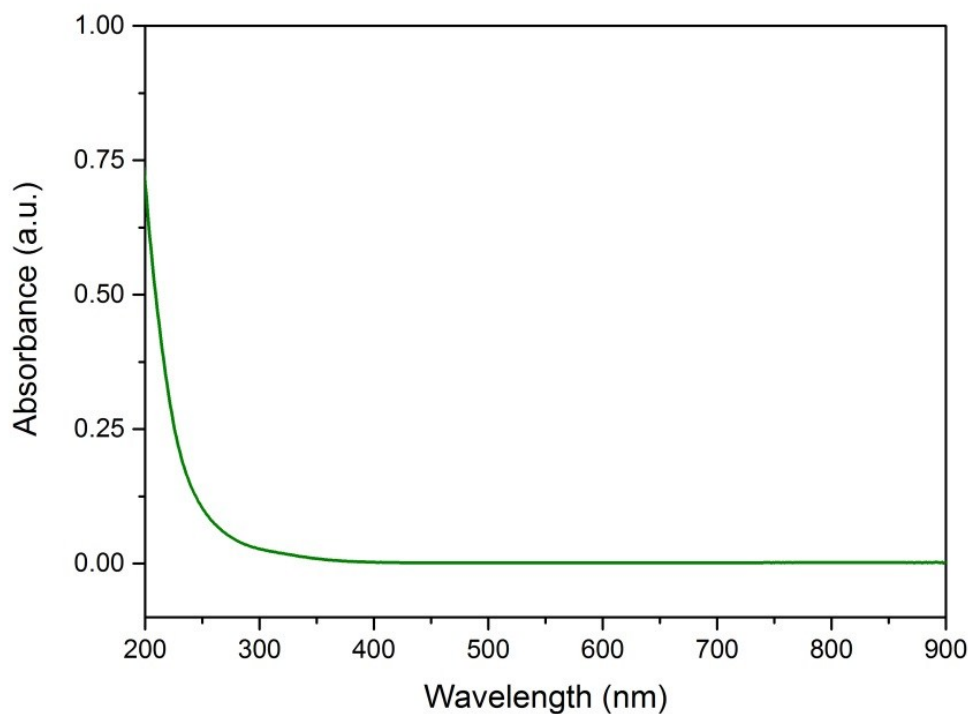


Figure S23. Optical spectrum of the aqueous dispersions of the functionalized nanosheets derived from AlB_2 , showing high absorbance in the UV region.

8. COLLOIDAL STABILITY IN TERMS OF ZETA POTENTIAL VALUES

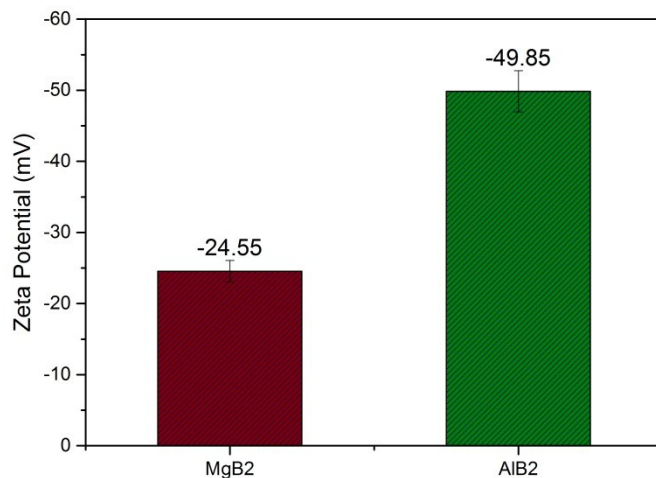


Figure S24. Comparing colloidal stability of nanosheets derived from MgB₂ and AlB₂ in terms of their Zeta potential values indicating the latter to be more stable.

Though the general mechanism remains the same for both the systems - MgB₂ and AlB₂, there are some differences observed when it comes to the finer details concerning the exfoliation of both compounds. For example, there is no vigorous gas evolution upon reacting aqueous solution of EDTA with AlB₂, unlike the case of MgB₂ wherein a visible froth layer forms on top of the reaction mixture for the initial hour of mixing. This has implications in the nanosheets' morphology as evident from the FESEM images: while MgB₂ derived sheets have typical perforations, these are absent in the case of AlB₂. There is a sol gel formation with time in the residues after exfoliation of AlB₂ while the MgB₂ residues remain the same for up to an year. The metal atom extraction efficiency is much higher for the case of AlB₂ as indicated by the ICP-AES results. The colloidal stability of the nanosheets derived from AlB₂ has higher stability in terms of Zeta potential values, than those from MgB₂ as shown above. We anticipate that such differences arise from the following points - (i) MgB₂ and AlB₂, though belonging to the same family of metal diborides have different bonding nature; they are reported to have 96.8% and 92% ionicity, respectively. (ii) The chelating agent EDTA has two-fold higher affinity for Al atoms than Mg atoms. (iii) Mg and Al belong to different groups in the periodic table and hence have possible differences in the chemical behavior. Hence, it is important to fine tune parameters like reaction time, reactant ratio etc. for each specific system to optimize the yield.

Section IV: Evidence for Exfoliation

In order to gather evidence about the interaction of the chelator molecules with the metal diboride crystals, how the selective extraction of intergallery metal atoms by the EDTA molecules affect the crystal structure and morphology, we performed XRD analysis and FESEM imaging of the chelant treated boride powders at two stages of the exfoliation process. The boride powders were collected immediately after the 1 hour reaction period with the aqueous Na_2EDTA solution and also after the 24 hour incubation period.

The chelant treated samples were recovered from the reaction mixture by centrifugation as follows: 15 ml sample was collected from the reaction mixture, centrifuged at 7500 rpm for 30 minutes at 4°C to let the boride powder settle to the bottom, the settled part was frozen and then lyophilized to obtain dry treated boride powder.

The following figures depict the XRD patterns and FE-SEM images of the treated MgB_2 and AlB_2 samples prepared as above as well as the standard metal boride powders.

1. XRD AND FE-SEM STUDIES ON CHELANT TREATED MgB_2 SAMPLES

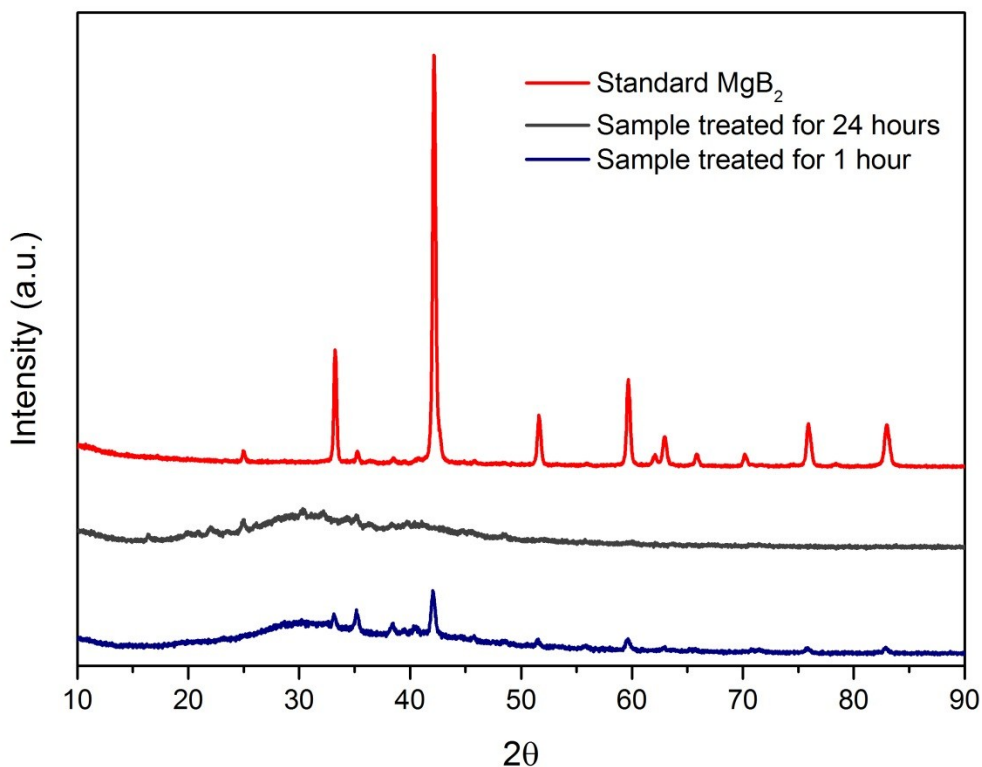


Figure S25. XRD patterns of standard MgB_2 , MgB_2 immediately after reaction with Na_2EDTA , and MgB_2 after reaction with Na_2EDTA for 24 hours.

As seen from the XRD patterns, standard MgB_2 has peaks corresponding to the (001) basal plane at $2\theta=25^\circ$ and the (002) plane at $2\theta=51.6^\circ$. The peaks corresponding to these planes in the treated

powders give us an idea about the effect of the chelant treatment on B-B planes and Mg-Mg planes, respectively. The “after 1 hour” sample shows the peak corresponding to the (002) planes, but it is absent in the “after 24 hours” sample; this can be attributed to the damage incurred by the Mg planes because of the substantial loss of Mg atoms from the inter gallery spaces upon prolonged chelant exposure. This is further corroborated by the FE-SEM images of these samples, wherein we can see indications of interlayer excavations corresponding to Mg loss in samples treated for 24 hours. FESEM-EDX results (Figure S24 e) also confirm the loss of Mg from the chelant treated borides as compared to the parent MgB_2 . The peak for (001) has slightly shifted to the left for the sample after 24 hours treatment compared to standard MgB_2 ; this could be due to the expansion occurring between the B-B planes due to functionalization derived from the aqueous ambiance owing to Mg loss. A similar analysis for the sample immediately after the 1 hour treatment could not be made conclusively because as evident from the XRD pattern it does not display the (001) peak. The MgB_2 -chelant mixture was very reactive for the first few hours and it was challenging to recover the treated boride powder as once it was extracted from the mother reaction solution, some degradative side reactions started occurring. This might have caused damage to the boron planes in the “after 1 hour” sample.

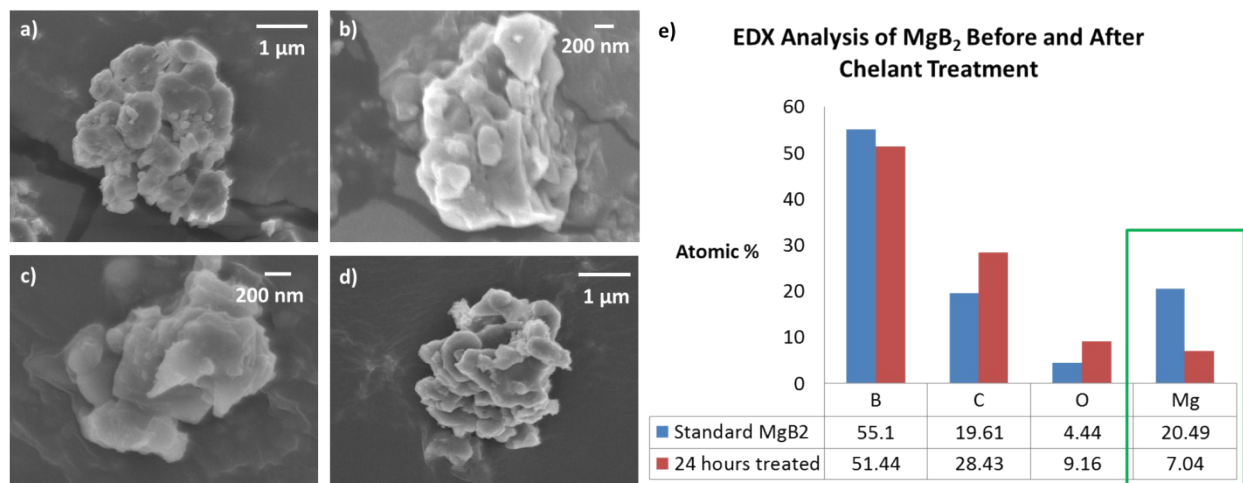


Figure S26. FE-SEM images of - (a) standard magnesium boride powder; (b-d) sample after 24 hour incubation (settling) period after the one hour mixing in aqueous Na_2EDTA solution showing inter layer excavations; (e) EDX results comparing the chemical composition of the MgB_2 powder before and after chelant treatment, showing loss of Mg in the treated samples due to chelation with EDTA.

2. XRD AND FE-SEM STUDIES ON CHELANT TREATED AlB_2 SAMPLES

The following XRD patterns and FE-SEM images have been obtained for treated AlB_2 powders and the standard aluminium diboride powder.

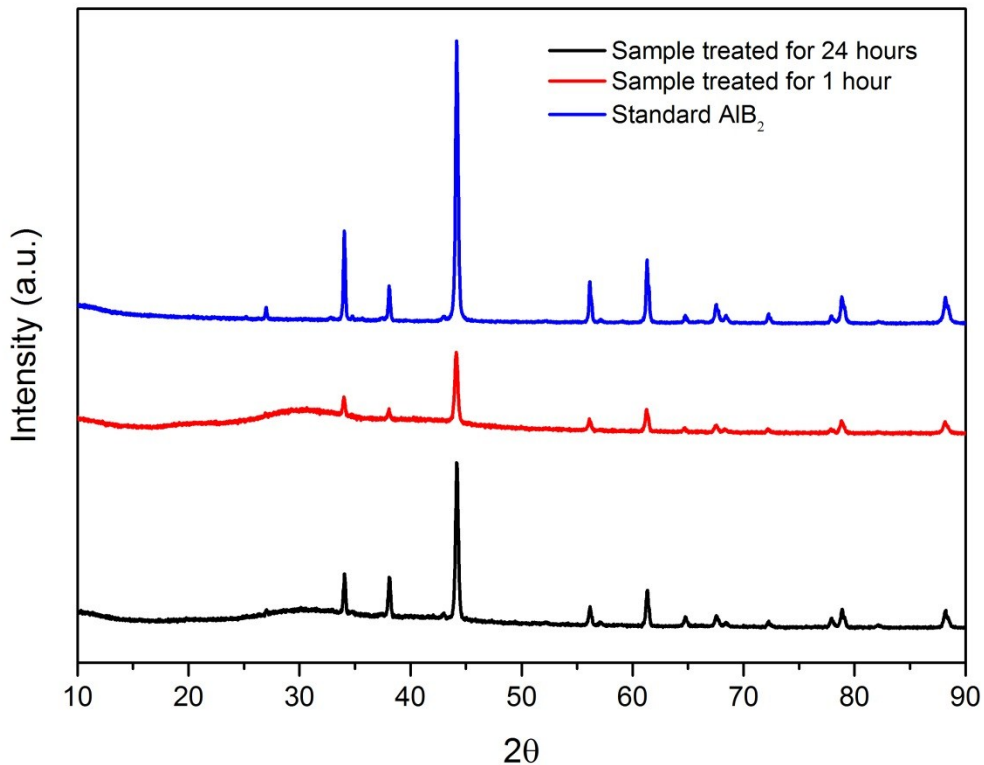


Figure S27. XRD patterns of standard AlB_2 , AlB_2 immediately after reaction with Na_2EDTA , and AlB_2 after reaction with Na_2EDTA for 24 hours.

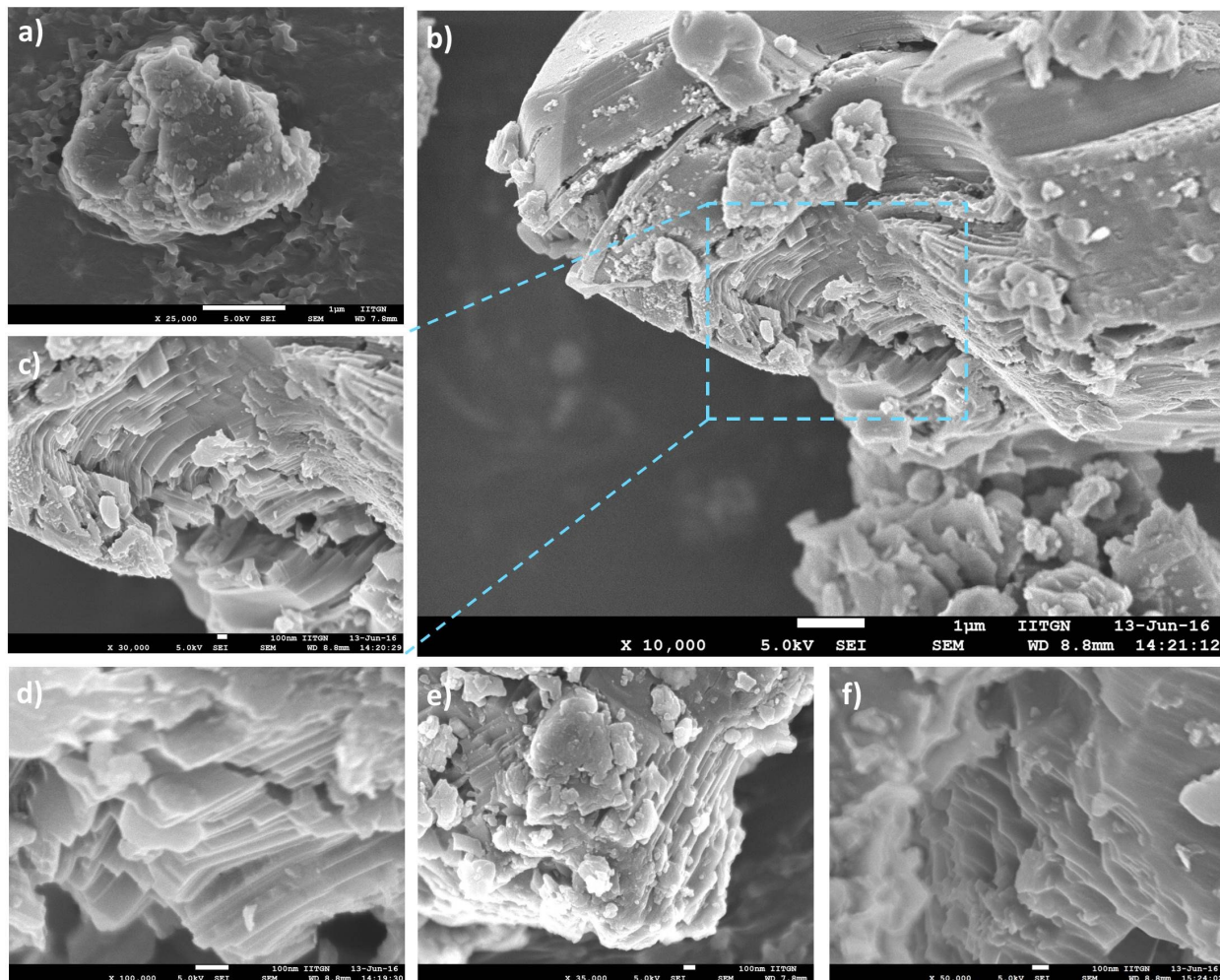


Figure S28. FE-SEM images of - (a) standard aluminium boride powder; (b-e) sample immediately after the one hour mixing period in 0.1M Na₂EDTA solution; (c) is the zoomed part marked in the large crystal shown in panel *b* indicating the interlayer gaps due to Al loss; (f) sample after 24 hour incubation (settling) period after the one hour mixing.

3. TEM IMAGES OF CONTROL EXPERIMENT: MgB₂ MIXED WITH WATER

We had attempted running control experiments to eliminate the possibility that few-layer-thick nanosheets might be present in the bulk material and just mixing in a solvent could aid in their dispersion. We performed this experiment by mixing MgB₂ in water for 1 hour and incubating it at ambient temperature for 24 hours, similar to the synthesis step for chelation assisted exfoliation. The clear top part of the settled suspension was recovered by centrifugation. The hence obtained supernatant solution was deposited on a lacey carbon Cu grid and imaged under TEM. The TEM images revealed structures as shown below. The structures are spherical particles of ~1 μm diameter or fused particles and do not resemble the nanosheets reported upon reaction with chelant. These may be the finer sized MgB₂ particles in the starting boride powder.

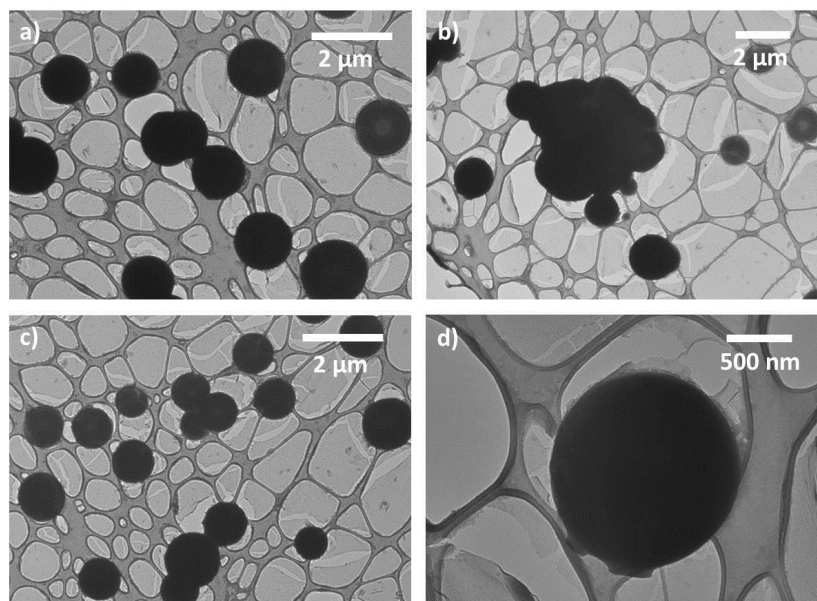


Figure S29. TEM images of supernatant from mixing MgB₂ and water depict micrometer sized particles that do not resemble nanosheets.

REFERENCES:

1. Garcia, A.; Raya, A. M.; Mariscal, M. M.; Esparza, R.; Herrera, M.; Molina, S. I.; Scavello, G.; Galindo, P. L.; Jose-Yacamán, M.; Ponce, A., Analysis of electron beam damage of exfoliated MoS(2) sheets and quantitative HAADF-STEM imaging. *Ultramicroscopy* **2014**, *146*, 33-38.
2. Cretu, O.; Lin, Y.-C.; Suenaga, K., Inelastic electron irradiation damage in hexagonal boron nitride. *Micron* **2015**, *72*, 21-27.
3. Gupta, S.; Hlova, I. Z.; Kobayashi, T.; Denys, R. V.; Chen, F.; Zavaliy, I. Y.; Pruski, M.; Pecharsky, V. K., Facile synthesis and regeneration of Mg(BH₄)₂ by high energy reactive ball milling of MgB₂. *Chemical communications (Cambridge, England)* **2013**, *49* (8), 828-30.
4. Pistidda, C.; Garroni, S.; Dolci, F.; Bardají, E. G.; Khandelwal, A.; Nolis, P.; Dornheim, M.; Gosalawit, R.; Jensen, T.; Cerenius, Y.; Suriñach, S.; Baró, M. D.; Lohstroh, W.; Fichtner, M., Synthesis of amorphous Mg(BH₄)₂ from MgB₂ and H₂ at room temperature. *Journal of Alloys and Compounds* **2010**, *508* (1), 212-215.
5. Turner, G. L.; Smith, K. A.; Kirkpatrick, R. J.; Oldfield, E., Boron-11 nuclear magnetic resonance spectroscopic study of borate and borosilicate minerals and a borosilicate glass. *Journal of Magnetic Resonance (1969)* **1986**, *67* (3), 544-550.
6. Alarco, J. A.; Chou, A.; Talbot, P. C.; Mackinnon, I. D. R., Phonon modes of MgB₂: super-lattice structures and spectral response. *Physical Chemistry Chemical Physics* **2014**, *16* (44), 24443-24456.
7. Awana, V. P. S.; Vajpayee, A.; Mudgel, M.; Ganesan, V.; Awasthi, A. M.; Bhalla, G. L.; Kishan, H., Physical property characterization of bulk MgB₂ superconductor. *Eur. Phys. J. B* **2008**, *62* (3), 281-294.
8. Ferrari, A. C.; Basko, D. M., Raman spectroscopy as a versatile tool for studying the properties of graphene. *Nat Nano* **2013**, *8* (4), 235-246.

9. Bateni, A.; Erdem, E.; Repp, S.; Acar, S.; Kokal, I.; Häföler, W.; Weber, S.; Somer, M., Electron paramagnetic resonance and Raman spectroscopy studies on carbon-doped MgB₂ superconductor nanomaterials. *Journal of Applied Physics* **2015**, *117* (15), 153905.
10. Motaman, A.; Hossain, M. S. A.; Xu, X.; See, K. W.; Chung, K. C.; Dou, S. X., A comprehensive study of the pinning mechanisms of MgB₂ wires treated with malic acid and their relationships with lattice defects. *Superconductor Science and Technology* **2013**, *26* (8), 085013.
11. Rafailov, P. M.; Bahrs, S.; Thomsen, C., The Raman Spectra of MgB₂ and Its Potential Impurity Phases. *physica status solidi (b)* **2001**, *226* (2), R9-R11.
12. Yates, K. A.; Burnell; Stelmashenko, N. A.; Kang, D. J.; Lee, H. N.; Oh, B.; Blamire, M. G., Disorder-induced collapse of the electron-phonon coupling in MgB₂ observed by Raman spectroscopy. *Physical Review B* **2003**, *68* (22), 220512.
13. A.Talapatra; Bandyopadhyay, S. K.; Sen, P.; Barat, P.; Mukherjee, S.; Mukherjee, M., X-ray photoelectron spectroscopy studies of MgB₂ for valence state of Mg. *Physica C: Superconductivity and its Applications* **2005**, *419* (3–4), 141-147.
14. Garg, K. B.; Chatterji, T.; Dalela, S.; Heinonnen, M.; Leiro, J.; Dalela, B.; Singhal, R. K., Core level photoemission study of polycrystalline MgB₂. *Solid State Communications* **2004**, *131* (5), 343-347.
15. Yao, H. B.; Li, Y.; Wee, A. T. S., An XPS investigation of the oxidation/corrosion of melt-spun Mg. *Applied Surface Science* **2000**, *158* (1–2), 112-119.
16. Wu, Y. Y.; Zhao, F. Q.; Xu, S. Y.; Ju, X. H., Access to novel graphene-like sheet of hydroboron: first-principles investigation. *Chemistry, an Asian journal* **2015**, *10* (2), 362-9.
17. Das, S. K.; Bedar, A.; Kannan, A.; Jasuja, K., Aqueous dispersions of few-layer-thick chemically modified magnesium diboride nanosheets by ultrasonication assisted exfoliation. *Sci. Rep.* **2015**, *5*.